Journal of Materials Chemistry A

Accepted Manuscript

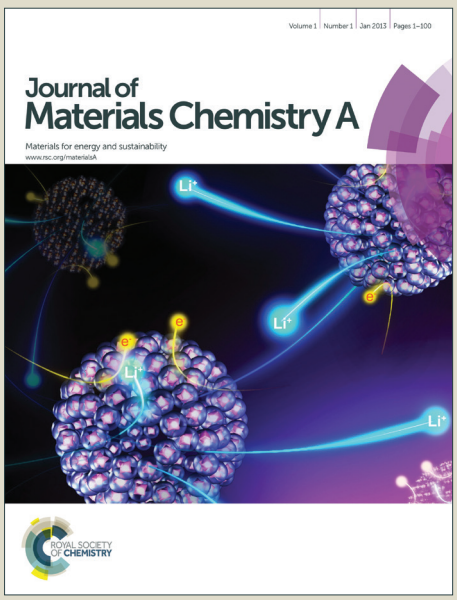

ROYAL SOCIETY OF CHEMISTRY

www.rsc.org/materialsA

Journal of Materials Chemistry A RSCPublishing

COMMUNICATION

A facile phase transformation method for the preparation of 3D flower-like β-Ni(OH)$_2$/GO/CNTs composite with excellent supercapacitor performance

Cite this: DOI: 10.1039/x0xx00000x

Received 00th January 2012,
Accepted 00th January 2012

DOI: 10.1039/x0xx00000x

www.rsc.org/

Xiaowei Ma,[a] Jiwei Liu,[b] Xiwen Gong,[a] and Renchao Che*[a]

3D flower-like β-Ni(OH)$_2$/GO/CNTs composite was prepared via a facile phase transformation method, with a high specific capacitance of ~1815 F g^{-1} (nearly 96% of its theoretical pseudocapacitance) at 2 A g^{-1} and a good cycling performance of ~97% capacitance retention after 2000 cycles at 10 A g^{-1}. The morphology of β-Ni(OH)$_2$ showed successive changes and could be controlled by adjusting the reaction time.

Nickel hydroxide is a promising electrode material due to its high theoretical capacity, well-defined redox behavior and potential applications in alkaline batteries and supercapacitors.[1] Up to now, considerable efforts have been devoted to controlling the morphology of Ni(OH)$_2$,[2] which greatly influences its electrochemical performance. Because its morphology can influence specific surface area, ion transport pathways and even conductivity, any of which is important to its electrochemical performance.[3] Moreover, the crystalline type of Ni(OH)$_2$ has remarkable influence on its electrochemical performance.

Ni(OH)$_2$ has two main crystalline types: α- and β-type.[4] α-Ni(OH)$_2$ consists of stacked Ni(OH)$_2$ layers with intercalated anions (such as nitrate and sulfate anions) and water molecules occupying the space between Ni(OH)$_2$ layers. β-Ni(OH)$_2$ has a hexagonal brucite-like structure and consists of close stacked Ni(OH)$_2$ layers without any intercalated species. α-Ni(OH)$_2$ displays more disorder and larger interlamellar distance. Compared with β-Ni(OH)$_2$, α-Ni(OH)$_2$ has much higher theoretical specific capacitance because its oxidation state can be +3.5 or even higher.[5] However, α-Ni(OH)$_2$ is unstable in alkaline solution because it easily transforms into β-Ni(OH)$_2$, leading to capacitance decay during electrochemical cycling process.[6] Although β-Ni(OH)$_2$ has relatively lower theoretical specific capacitance (~1892 F g^{-1} within a voltage window of 0.55 V, see Equation S1), it has better stability and higher discharge voltage, making it a promising electrode material. During the last decade, numerous efforts have been made to prepare high-performance electrode based on β-Ni(OH)$_2$, including β-Ni(OH)$_2$ grown on nickel foam[7] and β-Ni(OH)$_2$/graphene composites.[8] These strategies could enhance the electrical conductivity and effectively improved the electrochemical performance of the as-prepared electrodes. For example, β-Ni(OH)$_2$ nanoplates/graphene composites were reported, exhibiting high specific capacitance and excellent cycling performance.[8b] However, the previously reported β-Ni(OH)$_2$ nanoparticles grown on graphene or GO were mostly 2D nanoplates but hardly 3D nanostructures.

Herein, we report a facile phase transformation method to prepare 3D flower-like β-Ni(OH)$_2$ grown on GO. The special 3D morphology of Ni(OH)$_2$ could provide enough space and open channels for electrolyte penetration and rapid ion transport. The as-prepared 3D flower-like β-Ni(OH)$_2$/GO/CNTs composite exhibited high electrochemical performance with a specific capacitance of ~1815 F g^{-1} (based on the mass of Ni(OH)$_2$, nearly 96% of its theoretical specific capacitance) at 2 A g^{-1} within a voltage window of 0.55 V. Its cycling performance was also greatly improved and there was only a ~3% capacitance decay after 2000 cycles at 10 A g^{-1}.

The phase transformation from α-Ni(OH)$_2$ to β-Ni(OH)$_2$ could be accomplished within 1 h through a hydrothermal reaction in alkaline solution. The X-ray diffraction (XRD) peaks of the sample synthesized *via* a facile solvothermal reaction were in accordance with Ni(OH)$_2$•0.75H$_2$O (JCPDS No. 38-0715). Then the flower-like α-Ni(OH)$_2$ (400~500 nm) was transformed into β-Ni(OH)$_2$ after a hydrothermal reaction in alkaline solution (Fig. 1b). All the diffraction peaks could be well indexed to β-Ni(OH)$_2$ (JCPDS No. 14-0117). As the hydrothermal reaction time was increased from 1 h to 10 h, the full width at half maximum (FWHM) of the (101) peak at 38.5º became smaller (from 0.812º to 0.525º), indicating that the crystallinity and crystallite size increased with reaction time. As shown in Fig. 1c, the XRD patterns of Ni(OH)$_2$/GO/CNTs composites were similar to pure

$Ni(OH)_2$ samples, but a new peak at ~26° appeared, which corresponded to the (002) diffraction peak of carbon nanotubes (CNTs).[9]

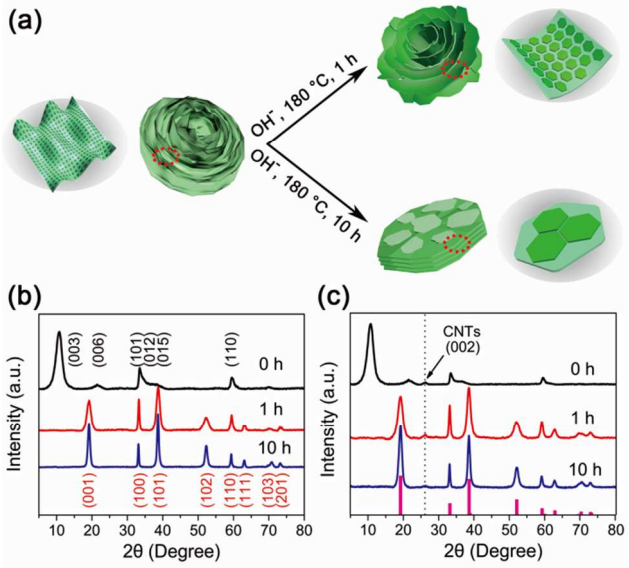

Fig. 1 (a) Schematic illustration of the transformation from α-$Ni(OH)_2$ to β-$Ni(OH)_2$ with successive morphological changes; (b) XRD patterns of as-prepared α-$Ni(OH)_2$ and samples after different hydrothermal reaction times: 1 h and 10 h; (c) XRD patterns of $Ni(OH)_2$/GO/CNTs composites. The standard data of β-$Ni(OH)_2$ are also shown for comparison.

Interestingly, the morphology of $Ni(OH)_2$ showed some remarkable changes as the hydrothermal reaction time was increased. There were three typical morphologies were characterized by scanning electron microscopy (SEM) and transmission electron microscopy (TEM): α-$Ni(OH)_2$ nanoflowers with distorted nanosheets, β-$Ni(OH)_2$ nanoflowers with smooth nanosheets and stacked β-$Ni(OH)_2$ nanosheets. Before hydrothermal reaction, the α-$Ni(OH)_2$ nanoflowers were spherical and their nanosheets exhibited distorted feature (Fig. 2a,b). After 1 h hydrothermal reaction in alkaline solution, the 3D flower-like morphology was mostly preserved with only a minor change that all the nanosheets of β-$Ni(OH)_2$ nanoflowers became smooth (Fig. 2c, d). The special 3D flower-like morphology could provide enough space and open channels for electrolyte penetration and rapid ion transport, which would be advantageous to its electrochemical performance.[10] As the hydrothermal reaction time was increased to 10 h, the product showed more significant changes: not only the nanosheets became much smoother, but also the nanoflowers were changed into stacked nanosheets as if they were compressed. Moreover, the nanosheets split into smaller ones (Fig. 2e and Fig. S2).

The preservation of 3D flower-like morphology should be attributed to the added alkali: NaOH. If no alkali were added, the dissolution process of α-$Ni(OH)_2$ would be faster than the crystallization process of β-$Ni(OH)_2$, resulting in serious destruction to the 3D flower-like morphology and the formation of single-crystalline hexagonal nanoplates as reported.[2a] When alkali was added, the dissolution process of α-$Ni(OH)_2$ was decelerated while the crystallization process of β-$Ni(OH)_2$ was accelerated. So the morphological change slowed down and the 3D flower-like morphology could be preserved.

Moreover, the morphology of β-$Ni(OH)_2$ showed successive morphological changes from 3D nanoflowers to stacked nanosheets. Crystallite size was suggested to be responsible for these morphological changes. The crystallite size of α-$Ni(OH)_2$ was ~4 nm estimated by the Scherrer equation from the (003) peak, while the crystallite sizes of two typical β-$Ni(OH)_2$ samples estimated from the (101) peak were ~8 and ~15 nm, respectively. Before hydrothermal reaction, the crystallite size of α-$Ni(OH)_2$ was quite small, which was beneficial to relax the strain induced by the distortion of nanosheets. After 1 h hydrothermal reaction, β-$Ni(OH)_2$ was obtained and its crystallite size was much larger, which could only relax little strain induced by the bend of nanosheets. As the crystallite size further increased, hardly any strain could be relaxed and only 2D flat nanosheets were obtained. Meanwhile, the thickness of nanosheets showed little change and was only few nanometers (Fig. S3). This was favorable for supercapacitor performance, because it could effectively shorten the ion diffusion length and enhance the utilization of electrode materials.[11]

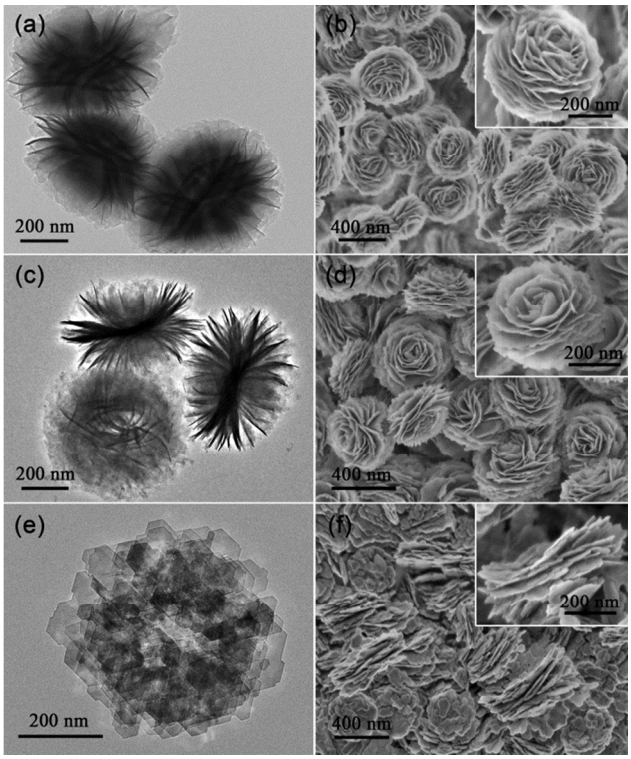

Fig. 2 (a, b) TEM and SEM images of α-$Ni(OH)_2$ nanoflowers before hydrothermal reaction. (c, d) TEM and SEM images of β-$Ni(OH)_2$ nanoflowers after a 1 h hydrothermal reaction. (e, f) TEM and SEM images of β-$Ni(OH)_2$ nanoflowers after a 10 h hydrothermal reaction.

It could be concluded that the added alkali had two main effects: (1) prevent β-$Ni(OH)_2$ from changing into planar nanoplates by influencing the phase transformation process; (2) cause the successive morphology changes by influencing the increase of crystallite size.

The successive morphology changes were also observed in $Ni(OH)_2$/GO/CNTs composites (Fig. 3). In our research, CNTs were used along with GO to enhance the electrical conductivity. CNTs could bridge the defects for electron transfer between GO nanosheets.[12] There was no obvious aggregation of CNTs in obtained composites (Fig. 3). The weight content of CNTs and GO in β-$Ni(OH)_2$/GO/CNTs composites was ~12% (Fig. S4).

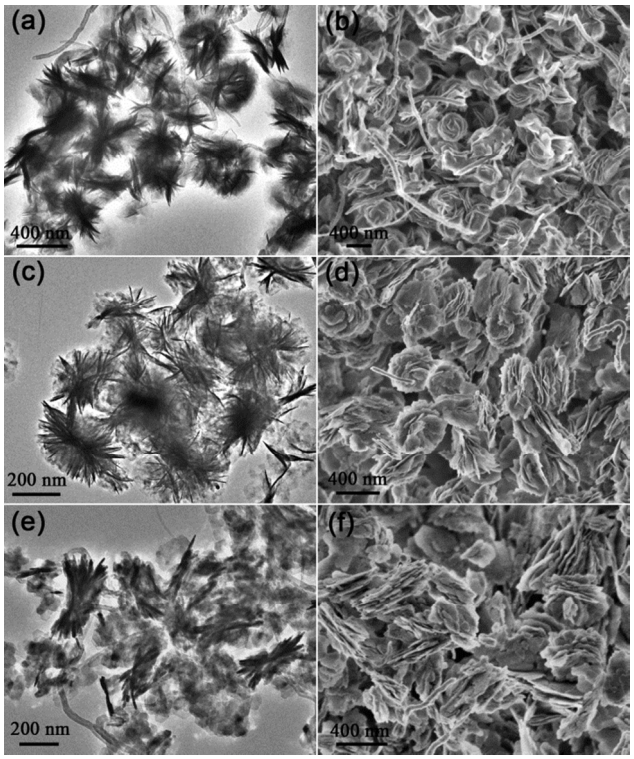

Fig. 3 (a, b) TEM and SEM images of α-$Ni(OH)_2$/GO/CNTs composite before hydrothermal reaction. (c, d) TEM and SEM images of β-$Ni(OH)_2$/GO/CNTs composite after a 1 h hydrothermal reaction. (e, f) TEM and SEM images of β-$Ni(OH)_2$/GO/CNTs composite after a 10 h hydrothermal reaction.

These as-prepared $Ni(OH)_2$/GO/CNTs composites with different morphologies showed quite different electrochemical performance. The specific capacitance of α-$Ni(OH)_2$/GO/CNTs was ~1511 F g^{-1} at 2 A g^{-1}, but only ~480 F g^{-1} at 20 A g^{-1} (based on the mass of $Ni(OH)_2$, Fig. 4a). It also suffered significant capacitance decay during cycling process (Fig. 4b). After about 600 cycles at 10 A g^{-1}, its specific capacitance decreased to ~454 F g^{-1}, only ~49% of the initial specific capacitance (~925 F g^{-1}). Its poor crystallinity and structural instability should be responsible for its poor electrochemical performance. In alkaline solution, α-$Ni(OH)_2$ could easily transform into β-$Ni(OH)_2$, resulting in structure and morphology changes.[13]

The 3D flower-like β-$Ni(OH)_2$/GO/CNTs composite obtained after 1h hydrothermal reaction showed greatly enhanced electrochemical performance. Its specific capacitance based on the mass of $Ni(OH)_2$ was ~1815, ~1435, ~1060, ~889 and ~857 F g^{-1} at 2, 5, 10, 15 and 20 A g^{-1}, respectively (Fig. 4a). Moreover, it exhibited greatly improved cycling performance. After 2000 cycles at 10 A g^{-1}, its specific capacitance was ~1028 F g^{-1} with only a ~3% capacitance loss.

As the hydrothermal reaction time was increased to 10 h, the morphology of β-$Ni(OH)_2$ changed into stacked nanosheets (Fig. 3e,f) and its crystallinity became better (smaller FWHM, Fig. 1c). The crystallinity of electrode material could influence its electrical conductivity and ionic conductivity, both of which are important to its electrochemical performance.[14] Although greater crystallinity can benefit the diffusion of protons in $Ni(OH)_2$, the β-$Ni(OH)_2$/GO/CNTs composite obtained after a 10 h hydrothermal reaction showed much lower specific capacitance based on the mass of $Ni(OH)_2$: ~1041, ~906, ~717, ~588 and ~511 F g^{-1} at 2, 5, 10, 15 and 20 A g^{-1}, respectively (Fig. 4a). This probably was caused by its stacked morphology and splitting into smaller nanosheets which may influence the ion diffusion and electron transfer. These results indicated that both crystallinity and morphology were crucial to electrochemical performance.

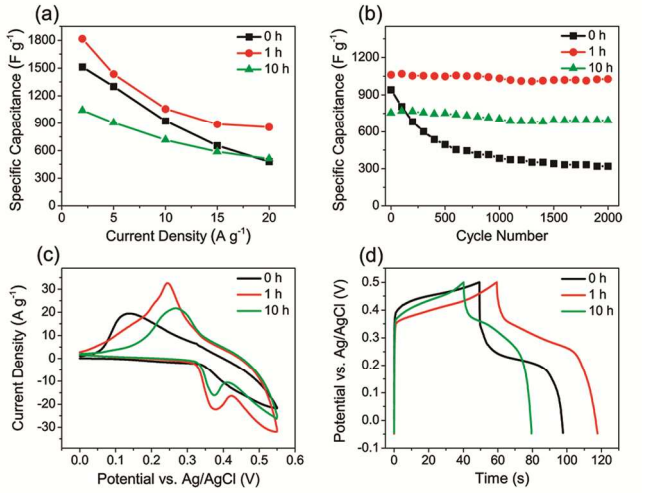

Fig. 4 Electrochemical characterizations of three selected samples (black, red and green lines correspond to the $Ni(OH)_2$/GO/CNTs composites after 0, 1 and 10 h hydrothermal reaction, respectively): (a) Average specific capacitances at various current densities; (b) Cycling performance at 10 A g^{-1}; (c) CV curves at 10 mV s^{-1}; (d) Galvanostatic charge/discharge curves at 10 A g^{-1}.

As shown in Fig. 4d, the discharge voltage plateaus of α-$Ni(OH)_2$/GO/CNTs was ~0.22 V (vs. Ag/AgCl). The lower discharge voltage would result in lower energy density (see Equation S2). β-$Ni(OH)_2$/GO/CNTs samples showed much higher discharge voltage plateaus around 0.30 V (vs. Ag/AgCl). Even if their specific capacitances were equal, the energy density of β-$Ni(OH)_2$ would be much higher than that of α-$Ni(OH)_2$.

The main energy storage mechanism of $Ni(OH)_2$ in alkaline solution is based on the following reversible redox reaction:

$$Ni(OH)_2 + OH^- \leftrightarrow NiOOH + H_2O + e^- \quad (1)$$

The change of the average oxidation state of Ni caused by the Faradic reaction can be detected by *ex situ* electron energy loss spectroscopy (EELS). There are two nickel excitation edges L_3 and L_2, corresponding to the electron transitions from $2p_{3/2}$ to $3d_{3/2}$, $3d_{5/2}$ and from $2p_{1/2}$ to $3d_{3/2}$, respectively.[15] Both the chemical shift of L_3 and the integral intensity ratio of white line

L_3/L_2 are sensitive to the oxidation state of transition metals: (a) absorption edges generally shift to higher energy with increased oxidation state; (b) L_3/L_2 ratio generally decreases with increased oxidation state.[16] The 3D flower-like β-$Ni(OH)_2$/GO/CNTs composite was selected as the research object. After charged at 10 A g^{-1}, the EELS spectrum of Ni showed a much higher L_3/L_2 ratio and a chemical shift of L_3 to higher energy compared with the sample before tested (Fig. 5a), indicating the average oxidation state of Ni was higher than +2.0.[17] However, after discharged at 10 A g^{-1}, the average oxidation state of Ni was still higher than +2.0, indicating the existence of residual Ni(Ⅲ).

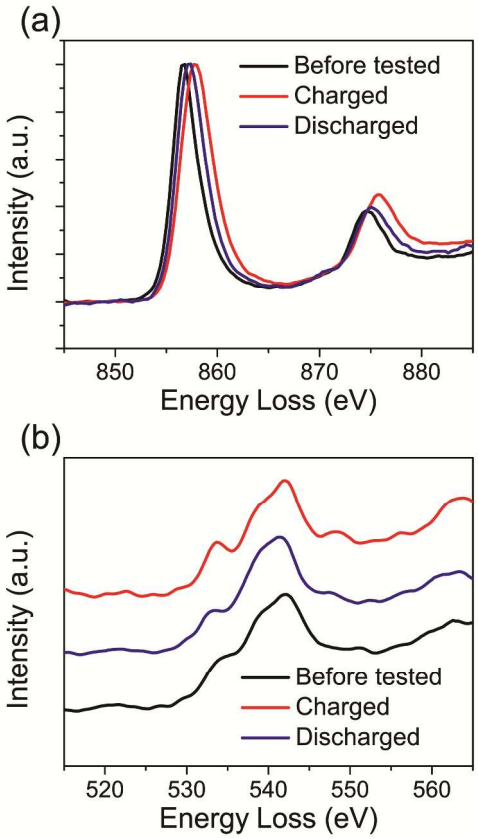

Fig. 5 EELS spectra of the sample after 1 h hydrothermal reaction: (a) Ni L edges and (b) O K edges obtained from samples before tested (black), after charged (red) and discharged (blue) at 10 A g^{-1}.

Moreover, the hybridization for O atoms was changed due to the generation of O^{2-} during the charging process. The O K edges were composed of a prepeak (~532 eV) and a broad edge (~540 eV) region. The prepeak intensity of O K notably increased after the sample charged at 10 A g^{-1} (Fig. 5b), revealing the remove of H atoms and the formation of O^{2-}.[17] After discharged at 10 A g^{-1}, the O K prepeak intensity still higher than that of the sample before tested. All these EELS data confirmed that the oxidation state change from Ni(Ⅱ) to Ni(Ⅲ) during charging process and the incomplete reduction of Ni(Ⅲ) during discharging process at 10A g^{-1}.

In summary, we developed a facile phase transformation method to prepare β-$Ni(OH)_2$ (and its composites) from α-$Ni(OH)_2$ nanoflowers with 3D flower-like morphology preserved. Successive morphological changes were observed during the hydrothermal reaction. The 3D morphology of the as-prepared β-$Ni(OH)_2$ could provide enough space and open channels for electrolyte penetration and rapid ion transport benefiting pseudocapacitive performance. Among the obtained composites with three typical morphologies, the 3D flower-like β-$Ni(OH)_2$/GO/CNTs composite showed the highest performance: both highest specific capacitance (~1815 F g^{-1} at 2 A g^{-1}) and best cycling performace (almost 97% capacitance retention after 2000 cycles at 10 A g^{-1}). This synthetic strategy could be applied to synthesis of other metal hydroxides with hierarchical morphology.

Notes and references

[a] Department of Materials Science and Laboratory of Advanced Materials, Fudan University, Shanghai, 200433, People's Republic of China.
[b] National Institute for Materials Science (NIMS), 1-2^{-1} Sengen, Tsukuba, Ibaraki, 305-0047, Japan.

† Electronic Supplementary Information (ESI) available: Supplementary SEM images, TEM images, TG curves, CV curves and charge/discharge curves are included. See DOI: 10.1039/c000000x/

1 G.-W. Yang, C.-L. Xu and H.-L. Li, *Chem. Commun.*, 2008, 6537.
2 (a) H. Wang, J. T. Robinson, G. Diankov and H. Dai, *J. Am. Chem. Soc.*, 2010, **132**, 3270; (b) J. W. Lee, T. Ahn, D. Soundararajan, J. M. Ko and J.-D. Kim, *Chem. Commun.*, 2011, **47**, 6305; (c) B. P. Bastakoti, H.-S. Huang, L.-C. Chen, K. C. W. Wu and Y. Yamauchi, *Chem. Commun.*, 2012, **48**, 9150; (d) H. Jiang, T. Zhao, C. Li and J. Ma, *J. Mater. Chem.*, 2011, **21**, 3818; (e) H. Jiang, C. Li, T. Sun and J. Ma, *Chem. Commun.*, 2012, **48**, 2606.
3 P. Simon and Y. Gogotsi, *Nat. Mater.*, 2008, **7**, 845.
4 P. Oliva, J. Leonardi, J. F. Laurent, C. Delmas, J. J. Braconnier, M. Figlarz, F. Fievet and A. d. Guibert, *J. Power Sources*, 1982, **8**, 229.
5 X.-P. Gao and H.-X. Yang, *Energy & Environmental Science*, 2010, **3**, 174.
6 G. Hu, C. Li and H. Gong, *J. Power Sources*, 2010, **195**, 6977.
7 (a) Y. Wang, D. Cao, G. Wang, S. Wang, J. Wen and J. Yin, *Electrochim. Acta*, 2011, **56**, 8285; (b) Z. Lu, Z. Chang, W. Zhu and X. Sun, *Chem. Commun.*, 2011, **47**, 9651.
8 (a) B. Li, H. Cao, J. Shao, H. Zheng, Y. Lu, J. Yin and M. Qu, *Chem. Commun.*, 2011, **47**, 3159; (b) H. Wang, H. S. Casalongue, Y. Liang and H. Dai, *J. Am. Chem. Soc.*, 2010, **132**, 7472.
9 C. Yuan, L. Chen, B. Gao, L. Su and X. Zhang, *J. Mater. Chem.*, 2009, **19**, 246.
10 J. Jiang, Y. Li, J. Liu, X. Huang, C. Yuan and X. W. Lou, *Adv. Mater.*, 2012, **24**, 5166.
11 G. Wang, L. Zhang and J. Zhang, *Chem. Soc. Rev.*, 2012, **41**, 797.
12 C. Yuan, L. Yang, L. Hou, J. Li, Y. Sun, X. Zhang, L. Shen, X. Lu, S. Xiong and X. W. Lou, *Adv. Funct. Mater.*, 2012, **22**, 2560.
13 G. A. Snook, N. W. Duffy and A. G. Pandolfo, *J. Power Sources*, 2007, **168**, 513.
14 S. Deabate, F. Henn, S. Devautour and J. C. Giuntini *J. Electrochem. Soc.*, 2003, **150**, J23.
15 (a) J. H. Paterson and O. L. Krivanek, *Ultramicroscopy*, 1990, **32**, 319; (b) C. Mitterbauer, G. Kothleitner, W. Grogger, H. Zandbergen,

B. Freitag, P. Tiemeijer and F. Hofer, *Ultramicroscopy*, 2003, **96**, 469.

16 (a) T. L. Daulton, B. J. Little, K. Lowe and J. Jones-Meehan, *J. Microbiol. Methods*, 2002, **50**, 39; (b) Z. L. Wang, J. S. Yin and Y. D. Jiang, *Micron*, 2000, **31**, 571.

17 Y. Koyama, T. Mizoguchi, H. Ikeno and I. Tanaka, *J. Phys. Chem. B*, 2005, **109**, 10749.

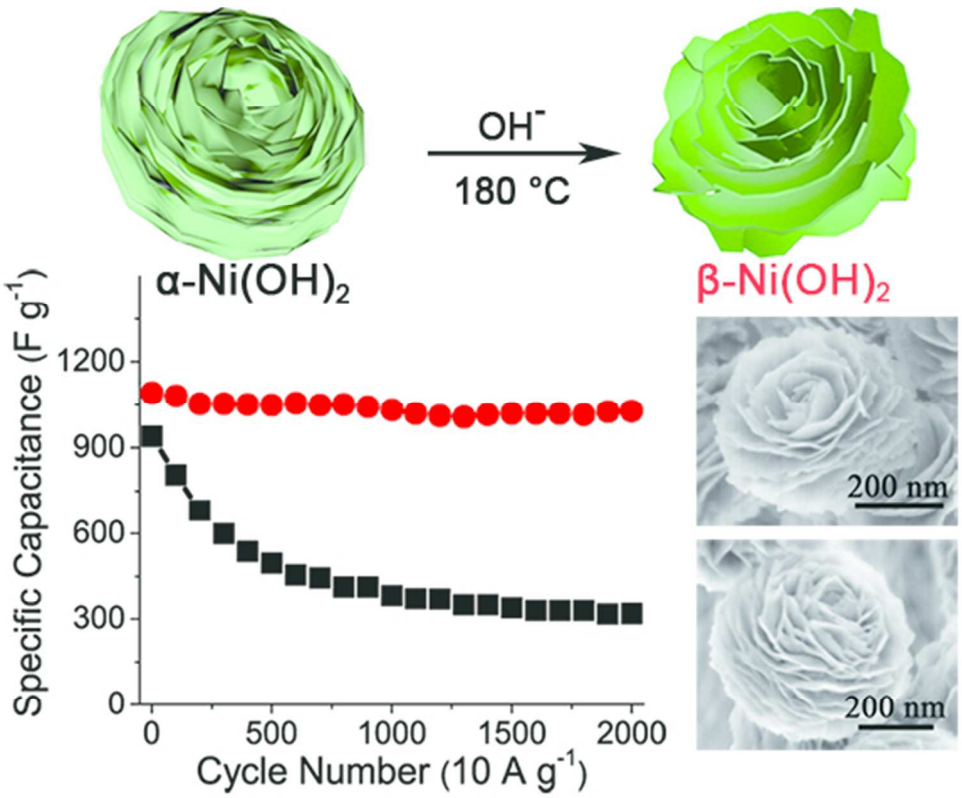

3D flower-like β-Ni(OH)2/GO/CNTs composite prepared via facile phase transformation method exhibited high specific capacitance (96% of theoretical pseudocapacitance at 2 A g-1) and good cycling performance (~97% capacitance retention after 2000 cycles at 10 A g-1). The morphology of β-Ni(OH)2/GO/CNTs showed successive changes and could be controlled by adjusting the reaction time.
50x39mm (300 x 300 DPI)